

INVESTIGATION OF THE SURFACE DEFORMATION AND DENDRITIC SOLIDIFICATION OF A TITANIUM ALLOY MELTED IN MILIGRAVITY

Authors:
Ms. Elena Sorina Lupu
Politechnic University of Bucharest, Romania, lupusorina@yahoo.com
Ms. Ioana Ciuca,
University of Durham, United Kingdom, ioana.ciuca@durham.ac.uk
Ms. Laura Manoliu,
Politechnic University of Bucharest, Romania, laura_mnl@yahoo.com
Ms. Claudia Chitu,
Politehnic University of Bucharest, Romania, chitu.claudia@yahoo.com
Mr. Claudiu Cherciu
Politechnic University of Bucharest, Romania, cherciu_claudiu@yahoo.com
Mr. Ion Ciobanu,
Politechnic University of Bucharest, Romania, ciobanu.nelu@hotmail.com
Mr. Camil Alexandru Muresan,
Politechnic University of Bucharest, Romania, murcamil@yahoo.com
Mr. Dan Dragomir,
Politehnic University of Bucharest, Romania, dan.dragomir@yahoo.com
Mr. Costel Nachila,
Politehnic University of Bucharest, Romania, nachila.costel@yahoo.com
Mr. Cristian Soare,
Politehnic University of Bucharest, Romania, soare.cristian@yahoo.com

Abstract

With the construction of the International Space Station, microgravity research has enabled many scientific breakthroughs. Moreover, new materials can be synthesized under low gravity conditions. In particular, in our analysis, an investigation on the surface deformation and on the dendritic solidification of a titanium alloy melted under Earth-based laboratory conditions and on board of a sounding rocket is performed [1]. This paper represents the first part of an ample research and is concerned with describing the rocket module platform [1] that will fly during the REXUS 15/16 campaign [2] from Kiruna, Sweden and the results obtained during the on-ground experiment. Also, it includes a detailed research regarding the hypothetical differences that will be obtained during the sub-orbital flight. The experiment contains a multimode LASER diode with an output power of 25 W that will melt samples Ti6Al4V covered with nanotubes. The nanotubular array is elaborated in Polyethylene glycol (PEG600). The research follows to understand the changes in microstructure, especially in the dendritic distribution. The results obtained under Earth conditions are presented in the Results section and then commented on the Discussion section. Here, we propose a comparative analysis with the results obtained under reduced gravity conditions (in the rocket), where we expect a difference in the dendrite geometry, particularly an increased spacing in the dendrites of an alloy that solidify in low gravity [3]. The paper also contains a mathematical model of the heat transfer mechanism that is purely diffusive. The second part of our research is concerned with the experiment on board of the rocket, when, during the 120 seconds of miligravity, the LASER is expected to melt the samples. The environmental parameters are going to be monitored using sensors and the melting process is recorded with a camera. In conclusion, we take into consideration the fact that the only parameter that differs between the on-ground and the on board of the rocket experiment shall be the level of gravity (the pressure, the temperature and the humidity must remain the same). So, a proficient comparison between the low and normal gravity effects can be undertaken.

1. Introduction

The heat and fluid flow occurring during laser treatment have an effect on the formation of the **microstructure** in a weld or melt. We are primarily interested in understanding how a certain grain structure forms as a result of solidification under reduced gravity conditions and also how this structure affects the mechanical properties. Our study starts by considering an analytical heat flow model in a material. Furthermore, the paper presents *the setup of the experiment and the results* on-ground, under normal conditions of pressure and temperature, with a link to the experiment that will fly on board of a sounding rocket (REXUS) from Kiruna, in 2014 (see Section Experiment Setup).

The chosen materials for our experiment are Ti6Al4V and acid core solder. However, the laboratory-based experiment was performed only with samples of

titanium alloy. We used a LASER with a maximum power of 25W to melt the metals.[1]For the rocket experiment, we will use the same LASER diode.

A SEM Inspect S, FEI Netherlands Electronic Microscope will be used to study the microstructure of the samples processed under both normal and reduced gravity conditions. This means a detailed investigation of the process microstructure, i.e. we will study the grain structure for the melt in the fusion zone (where the melting occurs) to see if we obtain a finer structure in reduced gravity or normal gravity. We will also investigate the heat-affected zone, where the microstructure is affected by the heat flow, and also the base metal. For the weld, an electronic microscope will be employed to study the process microstructure and the weld bead to see if there is a difference in the geometry of the grain structures that form in the alloy; observe how the microstructure varies across the fusion region, evolving from a planar structure near the boundary to a more complex structure (dendritic) near the centerline[2]. We will investigate the shape, the orientation and the spacing of the microstructures. For the weld bead, we will also study its geometry.

2. Theoretical Background

The temperature distribution in a material can be modeled by:[2]

$$\rho c_p \frac{dT}{dt} = \nabla \cdot (k \nabla T) + q_s \qquad [1]$$

Where ρ is the density, c_p is the specific heat temperature, T temperature, k is the thermal conductivity and q_s the rate of local energy generated per unit volume. For eq. [1] it has been assumed that the principal mechanism for heat flow in the material is conduction, and that there are negligible heat exchanges with the environment[2]. Eq. [1] can be derived using Fourier's law and the conservation of heat (heat absorbed = heat out – heat in) in a control volume. For the present study, we are more interested in the temperature distribution, which represents a solution of Eq. [1].

With the assumptions that k is invariant under temperature variations ($\frac{\partial k}{\partial T} = 0$), that q_s is insignificant (q_s=0) and that the material is homogenous (not our case, but it's a necessary simplifying assumption)[2], Eq. [1] becomes:

$$\rho c_p \frac{\partial T}{\partial t} = k \nabla^2 T \qquad [2]$$

Diffusivity is defined as:

$$\kappa = \frac{k}{\rho c_p} \qquad [3]$$

Eq. (2) becomes:

$$\frac{\partial T}{\partial t} = \kappa \nabla^2 T \qquad [4]$$

Let:

$$T = X(x)Y(y)Z(z)\tau(t), \qquad [5]$$

Where we have considered the temperature to be a function in three independent spatial variables: x, y, z and a time variable, t.[2]The origin of the (x, y, z, t) system is chosen to be the point at which the laser interacts with the material. We are modeling the laser to be a stationary instantaneous heat source.

In order to solve Eq. [4], we need to know the dimensionality and the boundary conditions imposed by it.

In order to solve [4] analytically we assume that no phase change occurs. Now, we analyze the heat flow in the three dimensions, that is, in the x, y and z directions. Once we have set the dimensionality of the flow, we have the boundary conditions:

$$\frac{\partial T}{\partial x} = 0 \text{ as x } \to \infty, \qquad [6]$$

since there is no temperature variation infinitely far away from the heat source.

Similarly:

$$\frac{\partial T}{\partial y} = 0 \text{ as y } \to \infty \qquad [7]$$

$$\frac{\partial T}{\partial z} = 0 \text{ as z } \to \infty \qquad [8]$$

The heat source can be modeled as a "contracting-to-a-line" cylinder, and we have a further boundary condition dependent on the radius of the cylinder, $r = \sqrt{x^2 + y^2 + z^2}$: when r goes to zero, the flux of the contracting cylinder approaches the input flux of heat, q. In mathematical form, this is a simple limit expressed as[2]:

$$\lim_{r \to 0} -4\pi r^2 \, k \frac{\partial T}{\partial t} = q, \qquad [9]$$

Let T be of the form[3]:

$$T = \frac{q}{8(\pi \kappa t)^{2/3}} e^{-r^2/4\kappa t} \qquad [10]$$

Indeed, when substituting for T in Eq. [4] and in the boundary conditions, we get the confirmation of our solution. However, a further necessary assumption needs to be chosen. The laser source needs to be considered a continuous heat source. We consider the integrating factor (the time-continuous contribution):

$$I = \int_0^t f(\xi) e^{\frac{-r^2}{4\kappa(t-\xi)}} \frac{d\xi}{(t-\xi)^{3/2}} \qquad [11]$$

In order to solve [12] analytically, we must make some simplifying assumption: we take f(ξ) to be the heat flux, q, which is a constant. This is our case with our CW laser. We then perform the usual change of variable:

$$\zeta = (t - \xi)^{-1/2} \qquad [12]$$

[1]http://www.oclaro.com/product_pages/BMU25A-9xx-01-R03.php

[2]Kannatey, E. (2009) *Principles of Laser Material Processing*, New Jersey: Wiley

[3]Steen, W. (1991) *Laser Material Processing,* London: Springer-Verlag

In [10], we solve for T using the integrating factor in [11] with [12]:

$$T = \frac{I}{8((\pi\kappa t)^{2/3}} \qquad [13]$$

$$T = \frac{q}{8(\pi\kappa t)^{2/3}} \int_0^t e^{\frac{-r^2}{4\kappa(t-\xi)}} \frac{d\xi}{(t-\xi)^{3/2}} \qquad [14]$$

We introduce the complementary error function with the argument x:

$$erfc(x) = \frac{2}{\sqrt{\pi}} \int_x^\infty e^{-t^2}\, dt \qquad [15]$$

Another substitution is now performed in Eq. [14]:

$$\text{Let } \varepsilon(\zeta) = \frac{r\zeta}{\sqrt{4\kappa}}, \quad [19]$$

We obtain:

$$T = \frac{q}{4\pi\kappa r} erfc(\varepsilon\left(t^{-\frac{1}{2}}\right)) \qquad [16]$$

Or, in the final form for our present analysis:

$$T = \frac{q}{4\pi\kappa r} erfc(\frac{rt^{-\frac{1}{2}}}{\sqrt{4\kappa}}). \qquad [17]$$

A plot for the temperature distribution is shown in Fig. 2 for titanium at 25 W and time t=1s.The temperature decreases as a function of both radius and time. Our plot refers to the decrease in temperature in terms of distance from the source origin. The heat distribution in the material characterizes the heat affected zone (HAZ).

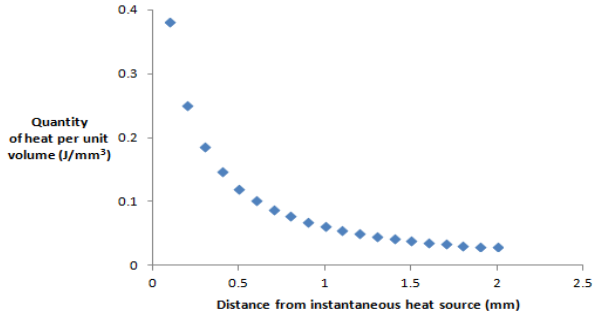

Fig. 1 Quantity of heat per unit volume of material in 3D flow for continuous stationary source

The rate at which a material cools after it has experienced high temperatures determines the grain structure that will form. The grain structure is an important indicator of the mechanical properties of the material. In our experiment, we study the solidification with fluid flow phenomena.

Fluid flow has an important role in the formation of the microstructure in the fusion zone. The forces that are responsible for fluid flow in the molten pool are buoyancy forces and surface tension forces.

SOLIDIFICATION WITH FLOW

We start by considering the governing equations for the fluid flow, with a special emphasis on Navier - Stokes equations, which express the dynamics of the flow.

The Navier-Stokes equations are dependent on force factors, implicitly on a gravitational factor. In order to make the equations more compact, let us consider the operators for a bidimensional analysis:

$$\nabla^2_{u_i} = \frac{\partial^2 u_i}{\partial x^2} + \frac{\partial^2 u_i}{\partial z^2} \qquad [18]$$

$$H_i = \frac{\partial u_i}{\partial t} + u_x \frac{\partial u_i}{\partial x} + \frac{\partial u_i}{\partial z} \qquad [19]$$

Assuming an incompressible fluid with negligible fluctuations in viscosity, we have the equations[2]:

$$\rho H_x = -\frac{\partial P}{\partial x} + \mu\nabla^2_{u_x} + F_x \qquad [20]$$

$$\rho H_z = -\frac{\partial P}{\partial z} + \mu\nabla^2_{u_z} + F_z \qquad [21]$$

Where F is the force vector, with components F_x, F_z (N/m3), P is the local fluid pressure (Pa) and μ is the dynamic viscosity (Pa s).

In material processing, the only force that has an effect is the gravitational force. That is $F_x = 0$ and F_z becomes, according to the Boussineq approximation[2]:

$$F_z = -\rho g \beta_T (T - T_0) + \beta_C (C - C_0) \qquad [22]$$

Where g is the gravitational acceleration, β_T is the volumetric thermal coefficient of expansion (/K) and β_C is the solutal volume expansion coefficient (/ %), T is the temperature and C is the concentration (the reference values are indexed with a 0).

DENDRITIC GROWTH

An important part in our experiment is the characterization of the zone that forms after solidification. In this respect, we investigate the geometry of dendrites, the small-size grain structures that form in alloys.

The dynamical equations that determine the formation of dendrites are similar to [20], [21], however, an adjacent term accounting for the permeability of the medium emerges.

The equations are[2]:

$$\rho H_x = -\frac{\partial P}{\partial x} + \nabla \cdot \left(\mu_l \frac{\rho}{\rho_l} \nabla u_x\right) - \frac{\mu_l}{K_p} \frac{\rho}{\rho_l} u_x \qquad [23]$$

$$\rho H_z = -\frac{\partial P}{\partial z} + \nabla \cdot \left(\mu_l \frac{\rho}{\rho_l} \nabla u_z\right) - \frac{\mu_l}{K_p} \frac{\rho}{\rho_l} u_z - \rho g \beta_T (T - T_0) + \beta_C (C - C_0) \qquad [24]$$

Where K_p is the permeability and is assumed to be isotropic1. The Caman-Kozeny equation models K_p, as given in Kannatey[2].

The enthalpy and solute concentration equations give important insights in the behavior of the molten pool, however, for our present study, the emphasis is put on the dynamical equations, in which the gravitational effect can be traced.

For the titanium melt, we expect a difference in the dendrite morphology since of the absence of buoyancy effects; we should see an increased spacing in the dendrites after having solidified in reduced gravity[4]. Furthermore, we will investigate if the weld shape is

formed flatly in a miligravity environment[4] and study the impact of gravity on its formation.

SURFACE TENSION EFFECT; MARANGONI CONVECTION

Surface tension varies with temperature. This induces a surface tension gradient along the surface that creates a tendency for the fluid to move to regions of higher surface tension. This flow is known as Marangoni convection.

The dynamical equations for Marangoni convection for a flat surface are[2]:

$$\mu \frac{\partial u_x}{\partial z} = -\frac{\partial T}{\partial x}\frac{\partial \gamma}{\partial T} \quad [25]$$

$$\mu \frac{\partial u_y}{\partial z} = -\frac{\partial T}{\partial x}\frac{\partial \gamma}{\partial T} \quad [26]$$

$$u_z = 0, \quad [27]$$

where γ is the surface tension of the molten pool at temperature T (J/m^2).

In their study "Thermocapillarity convection in a Model-Float Zone", Neitzel, Hyer and Jankowski used a finite-element method to model thermocapillarity convection in sodium nitrate corresponding to terrestrial microgravity body-force levels. Their results show that the isotherms obtained under microgravity conditions are more distorted than those obtained under terrestrial conditions. Furthermore, the thermocapillarity eddy appears to be more oval and less elongated than the one obtained on Earth[5]. Furthermore, in the microgravity experiment MKB (Marangoni Konvektion im offenen Boot) strong thermocapillarity flow was observed[6] in *Fig. 2 Thermocapillarity convection in MKB experiment*[6]

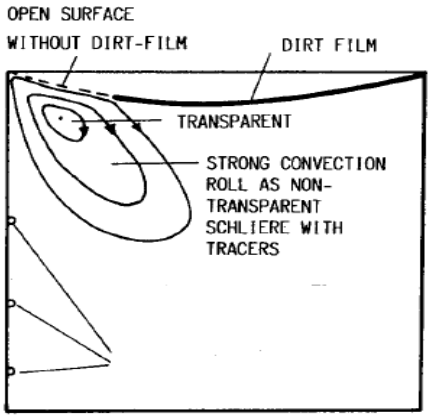

Fig. 2 Thermocapillarity convection in MKB experiment[6]

In the absence of gravity-driven convection, Marangoni convection can be studied properly. In our experiment, we look at the differences in the microstructure that arise as a result of intricate phenomena in the heat and fluid flow (Marangoni convection).

3. Experiment SETUP

OVERVIEW

The environmental parameters which affect materials processing are: gravity, temperature and pressure. The latter two can be controlled under laboratory conditions, but a gravity-controlled experiment is very difficult to obtain on Earth (drop towers can be used for this procedure). However, the duration of such an environment is not optimal for investigating materials processing. Given the fact that we will have a long period of miligravity environment in the REXUS rocket, we expect to get meaningful results.

ON-ROCKET EXPERIMENTAL SETUP

The experiment will contain a hermetically sealed 6061 aluminum alloy box of 223x223x180 mm, where the instruments are placed: the LASER and its driver, PCBs, sensors, LEDs, the optical system and the samples. The total mass of the experiment will be approximately 4 kg. (*Fig. 3 Experiment chassis*)

Fig. 3 Experiment chassis

The temperature and the time will be constantly measured and logged. In addition, pressure sensors, accelerometers and gyroscopes are used for in-situ measurements.

MELTED SAMPLES

Ti6Al4V will represent the main material used for melting and welding. Acid core solder will also be considered as a second alloy, because of its very low melting temperature. The samples will be mounted on a

[4]Nogi, K. *et al*. 1997, Solidification process in weld under microgravity, Proc.Int.Conf. HIGH TEMPERATURE CAPILLARITY

[5]Neitzel, G.P., Hyer, J.R., Jankowski, D. F. *"Thermocapillarity convection in a Model-Float Zone"*, 1990

[6]Schwabe, D. and Laprecht, R., *Marangoni Konvection im offenen Boot (MKB)*, 1986

frame that will shift slowly using a linear motor, as shown in the *Fig. 4 Experimental configuration*

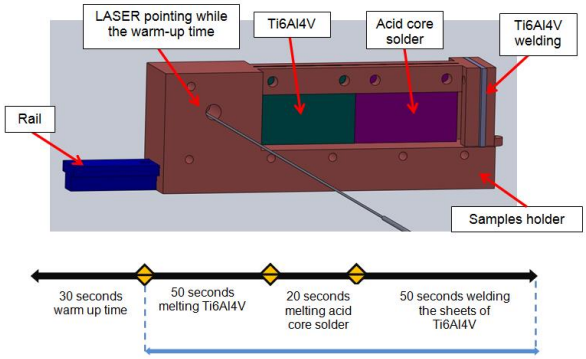

Fig. 4 Experimental configuration

The Ti6Al4V alloys are covered with carbon nanotubes in order to reduce the reflectivity and to increase absorption. The Ti6Al4V was obtained from the Institute of Management and System Technology, Bucharest, Romania. Surface pre-treatment involves: abrasion with silicon-carbide sandpaper of increased grit size (up to 4000 grit) until glossy smooth finish, cleaning and degreasing by successive 15 min ultrasonication steps in purified water, ethanol and acetone and thoroughly rinsed with tap and distilled water. The samples will be dried in air and used immediately. The creation of nanotubes is attained through an anodizing process. Anodization is carried out in a one compartment two-electrode electrochemical cell, having freshly conditioned Ti6Al4V piece as anode and Pt sheet as cathode. The electrochemical treatments consist of a potential sweep from 0 to 50 V with a 2 V/10 s step and then is kept constant at 50 V (total anodization time was 2 h at room temperature). A MATRIX MPS-7163 electrochemical source used to input the desired voltage. Anodizing in carried out in a hybrid inorganic and organic component as of polyethyleneglycoll + 2% v/v H2O + NH4F 0.5 wt%. After the treatment, the samples will be rinsed with purified water.

During the rocket flight, there will be approximately 120 seconds of miligravity of which, the first 50 seconds will be used to melt Ti6Al4V, the next 20 seconds to melt acid core solder and the last 50 seconds will be used to weld Ti6Al4V sheets. (as in *Fig. 4 Experimental configuration*)

The linear motor is controlled using a standard RC servomotor signal. We also have access to its potentiometer, in order to determine the actual position of the frame on the rail. This allows the microcontroller to determine the absolute position and take actions accordingly.

The experiment has a vibration damping system in order to reduce the high frequency vibrations that could affect the experiment during the flight and launch. The vibration damping system is composed of 2 rubber cylinders per bolt mounted in the exterior of the experiment.

We have chosen to use four A123 LiFePO4 batteries because they deliver high power and energy density but they also provide us with safety performance and they are rechargeable. They shall deliver 13.2 V.

In order to focus the laser beam at approximately 0.3 mm, there will be used two air-spaced doublet lenses. This will be attained by using a 2.1 X magnification configuration, obtained at a working distance of 60mm. The lenses are biconvex with 20mm focal length. The lens will be placed inside a connecting tube. An adaptor socket to accept a SMA fiber will be used. For our 915 nm wavelength range, we will use an appropriate antireflection coating (B coating) for the lens, in order to minimize the loss of incident light. The entire configuration is shown in *Fig. 5 Top View of the experiment and the rocket module* and *Fig. 6 Experiment Setup*.

The LASER diode will output a continuous wave and the maximum output power is 25W.

The electronics is divided into the MainBoard PCB and the LogBoard PCB. The first one connects to the REXUS interface, the experiment peripherals and sensors. The microcontroller on this board is able to take actions, communicate with the ground station, and send commands to all the devices. It must be able to work without the second electronics board, "LogBoard" whose main purpose is to log all the data.

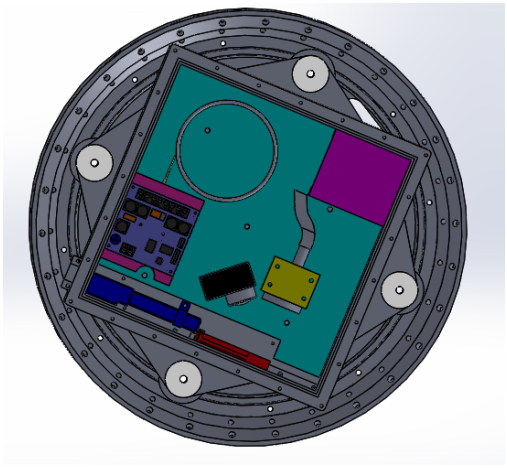

Fig. 5 Top View of the experiment and the rocket module

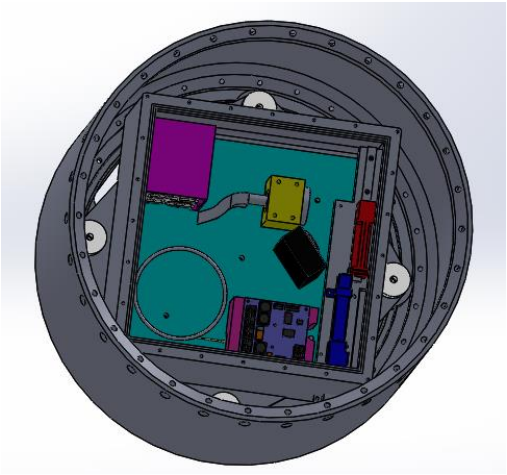

Fig. 6 Experiment Setup

Also, the only way the LogBoard depends on the mainboard is through the 5V power supply line. The MainBoard has external LEDs (on the electronics box) to indicate if the experiment has been powered on, a blinking

LED to indicate the microprocessor main software loop is working, and if the LASER driver has been enabled. Super-bright LEDs are also present in the experiment box to illuminate the metal samples. The Logboard uses an SD card to log all the experiment data: the motor position, the various temperatures, the battery voltage and LASER status.

Because of the thermal constrains (the rocket will stay in the launcher at -30°C) we need to use a heating element which will consist of a 20W resistor to heat up the LASER heat sink up to 15°C, and will only be powered on before Lift Off (LO) signal.

The experiment software consists of the Ground Station software, and the firmware running on the microcontrollers.

We will also use a GoPro 3 camera in order to record the phenomena which will occur during the flight and to analyze properly the welding and melting time. Regarding the temperature profile in the rocket when the laser is on, the simulation made in SOLIDWORKS software proved that the maximum temperature on the chassis will be in around 25 degrees, in the place where the laser is fixed. (the rocket constraints for the thermal were: "The thermal environment of the outer structure of a front-end positioned parallel bay module on an Improved Orion motor flight can reach 110°C at 50 seconds after lift-off", "After the impact, the payload will be subjected to snow and cold air in the impact area for a period of typically one to two hours.", "The temperature during the season when REXUS is launched is normally between 0°C and -30°C.", with the requirement that: "A module's internal thermal dissipation must not heat up parts facing other modules to more than +50°C.")[7].

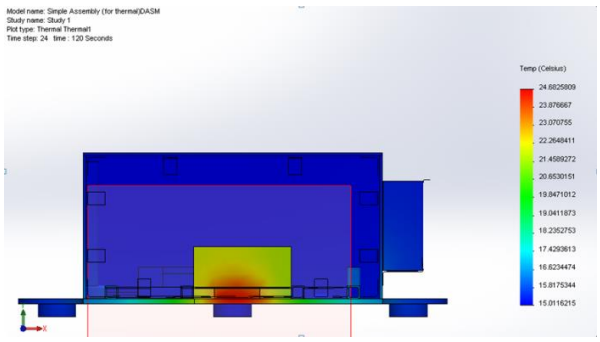

Fig. 7 Thermal Analysis

There will also be several tests regarding safety conditions and functionality: vibration, thermal, vacuum and over-pressure tests.

The entire experiment was designed and built considering the REXUS Manual. [7]

A similar experiment will be performed under Earth-based laboratory conditions, leading to a comparative analysis between the samples modified under low gravity conditions and in SATP environment.

THE ON-GROUND EXPERIMENT

The on-ground experiment was performed twice, at University of Durham and at Politehnica University of Bucharest. However, the analyzed samples presented in the Results Section are those from Polihnica University of Bucharest.

SETUP

The on-ground experiment was done in order to obtain relevant results in terms of the quality of melt of Ti6Al4V. The experimental setup was slightly different from the one that will be employed in the REXUS environment. It consisted of an aluminum heatsink, where we placed the laser, the optical fiber (bent at a radius of 3.75 cm), the optical system and the titanium sample at variable distances of mean 60 mm. We then used a RS232 serial to control the driver using PYTHON as the programming language.

In order to melt the titanium, we had to test the functionality of the laser and also determine whether at the focal distance of 60 mm quoted by the manufacturer of the optical system we indeed obtain the minimum spot size, i.e. the maximum energy density on the sample.

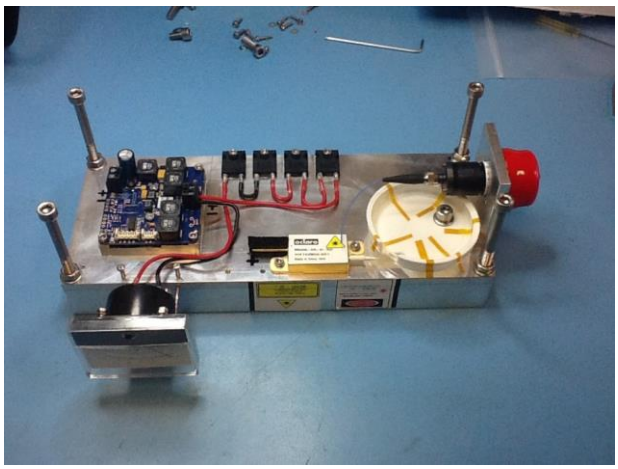

Fig. 8 On-ground configuration (University of Durham)

The difference between the predicted and the measured values are presented in *Table 1 Data acquisition from the laser diode*.

Table 1 Data acquisition from the laser diode

Output current from the diode (A)	PS Current (A)	Wattage predicted (W)	Wattage measured (W)
1	0.5	~ 1.5	~ 1.1
2	0.9	~ 4.0	~ 3.3
3	1.4	~ 7.0	~ 5.5
4	1.8	~ 10.0	~ 7.8
5	2.3	~ 12.5	~ 10.0
6	2.9	~ 15.0	~ 12.3
7	3.4	~ 17.5	~ 14.5
8	4.0	~ 20.0	~ 16.5
9	4.6	~ 23.0	~ 18.4
10	5.2	~ 25.0	~ 20.2

[7] http://www.rexusbexus.net/images/stories/rexus/RX_REF_user_manual_v7-7_06Sep12.pdf

After several experiments, as shown in *Table 1 Data acquisition from the laser diode*, we concluded that the optimal parameters for investigating the melt were found:

Table 2 Optimal parameters

Thickness	Power	Time	Distance
200 μm	20 – 25 W	50 s	60 ± 0.2mm

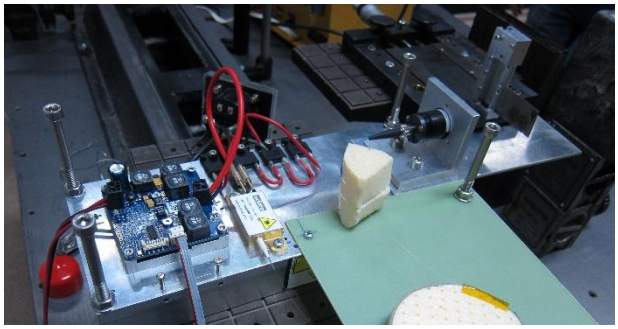

Fig. 9 Experiment at Politehnica University of Bucharest, Romania

MATERIAL PROCESSING BEFORE MELTING

Initial samples of Ti6Al4V were obtained by mechanical processing which involved cold-rolling deformation with a total reduction of 15.84 % (initial thickness of the sample was 1.2 mm).

The cold-rolling process was performed on a MARIO DI MAIO LQR120AS laboratory mill (rolling speed 1.5 m/min).

For the last two rolling steps, the billet roll stand has been pre-tensioned for a negative skip (- 0.2 mm).

In *Table 3 Cold-rolling scheme* is shown the cold-rolling scheme.

Table 3 Cold-rolling scheme

Rolling steps, i	**Thickness before rolling step h_{i-1}, [mm]**	**Thickness after rolling step hi, [mm]**	**Partial reduction ε_i, [%]**	**Total reduction ε_{tot}, [%]**
1	1.20	1.11	7.50	7.50
2	1.11	0.90	18.92	25.00
3	0.90	0.85	5.56	29.17
4	0.85	0.81	4.71	32.50
5	0.81	0.74	8.64	38.33
6	0.74	0.61	17.57	49.17
7	0.61	0.54	11.48	55.00
8	0.54	0.51	5.56	57.50
9	0.51	0.45	11.76	62.50
10	0.45	0.39	13.33	67.50
11	0.39	0.34	12.82	71.67
12	0.34	0.31	8.82	74.17
13	0.32	0.29	9.38	75.83
14	0.29	0.27	6.90	77.50
15	0.27	0.24	11.11	80.00
16	0.24	0.22	8.33	81.67
17	0.22	0.19	13.64	84.17

The mechanical processing was stopped at a thickness of 0.19 mm mainly due to the formation of the microcracks.

The formulae for partial reduction and total reduction are:

$$\varepsilon_i = \frac{h_{i-1}-h_i}{h_{i-1}} * 100\ [\%] \quad [25]$$

$$\varepsilon_{tot} = \frac{h_0-h_i}{h_0} * 100\ [\%] \quad [26]$$

Where h_0= 1.2 mm

MELTING PROCEDURES

Several samples of Ti6Al4V were mounted on an aluminum rail at 6 cm (focal point) from the optical system.

The table below emphasizes the melting process.

Table 4 Samples of Ti6Al4V melted on-ground

Sample	Material	Thickness (μm)	Power (W)	Time (s)	Distance from lens (mm)	Observation
A	Ti6Al4V	200	5.5	50	60 ± 0.2	HAZ
			10	50	60 ± 0.2	HAZ
B	Ti6Al4V	200	15	50	60 ± 0.2	HAZ
		300	15	50	60 ± 0.2	HAZ
C	Ti6Al4V	200	15	50	60 ± 0.2	HAZ
			20	50	60 ± 0.2	HAZ and hole
D	Ti6Al4V	200	20	30	60 ± 0.2	HAZ
			20	40	60 ± 0.2	HAZ

4. Results and discussion

The on-ground experiment was performed under normal conditions of temperature and pressure. Using the experiment setup presented in *Table 4 Samples of Ti6Al4V melted on-ground*, samples of Ti6Al4V were melted.

The Ti6Al4V samples were analyzed using three instruments: a Scanning Electron Microscope, an XRay Microtomograph and an Optical Microscope. Before SEM analysis, the samples were further

The figure below presents the samples immediately after the LASER interaction.

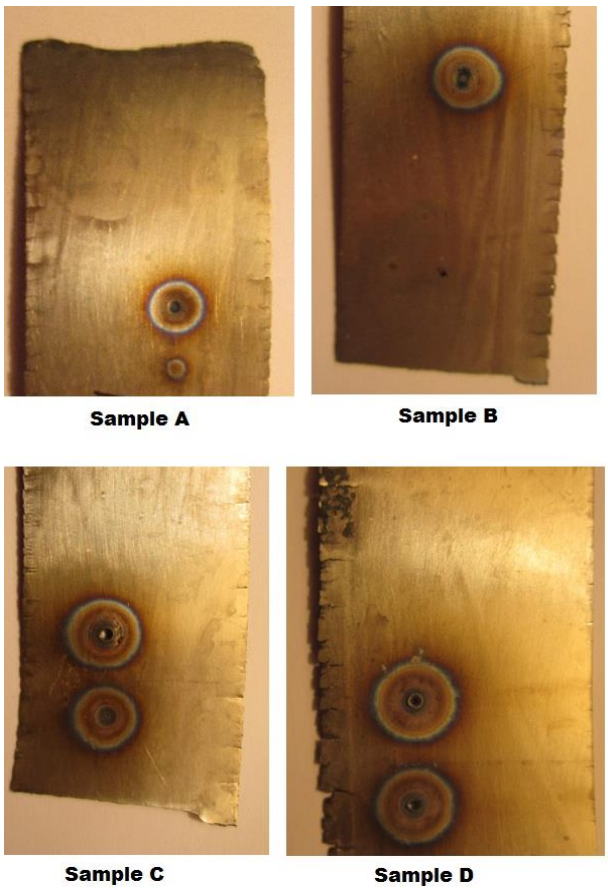

Fig. 10 Melt and HAZ

X-RAY MICROTOMOGRAPH

Using X-ray microtomograph, we were able to observe the micro-cracks formation due to the thermal effects (LASER interactions), as in *Fig. 11 Titanium alloy microcracks*.

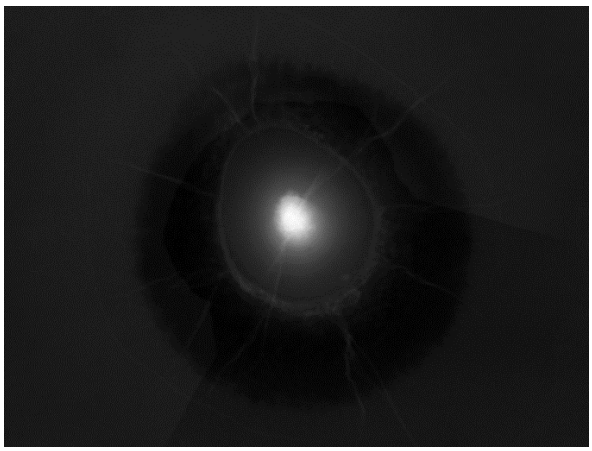

Fig. 11 Titanium alloy microcracks

The sample was exposed to 15W optical power during 50 minutes before XRAY analysis.

SCANNING ELECTRON MICROSCOPE

The sample was exposed to 20W during 50 minutes. Due to the thickness of the sample and the power of the LASER, a hole of 1 mm can be seen in *Fig. 12 LASER interaction with titanium*.

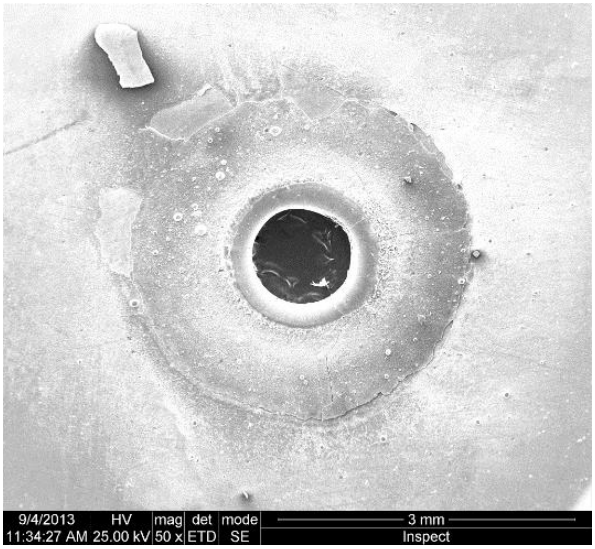

Fig. 12 LASER interaction with titanium

Furthermore, using the SEM, we were able to observe the dendritic pattern of the material (after and before LASER interaction). As can be seen in *Fig. 14 After LASER interaction*, their geometry is columnar on the largest scale. Their spacing is relevant on scales smaller than 100 µm. However, a detailed comparison needs to be undertaken after the REXUS flight in order to validate the differences in the spacing of dendrites. In *Fig. 15 Fusion zone*, the grain structures in the center of the fusion zone represent microporosities. The role gravity has in their formation is traceable in the shapes that can be seen; in miligravity we do not expect microporosities. Also, the shape of the fusion zone is a flattened meniscus as can be seen in Fig. 12; in miligravity, we expect its shape to be spherical.

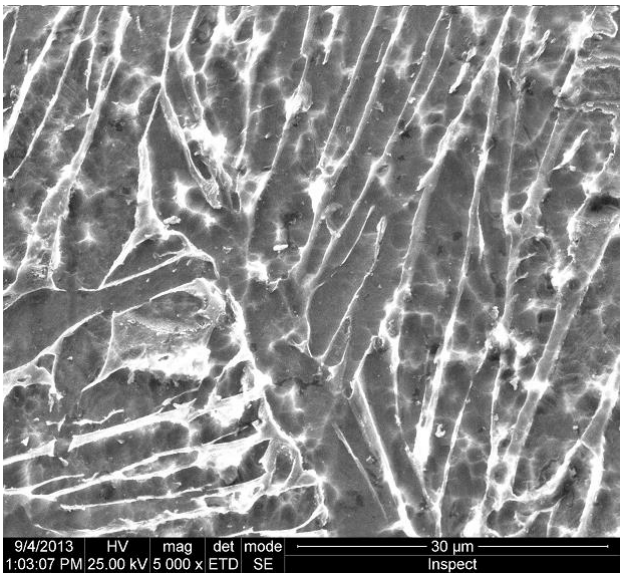

Fig. 13 Before LASER interaction

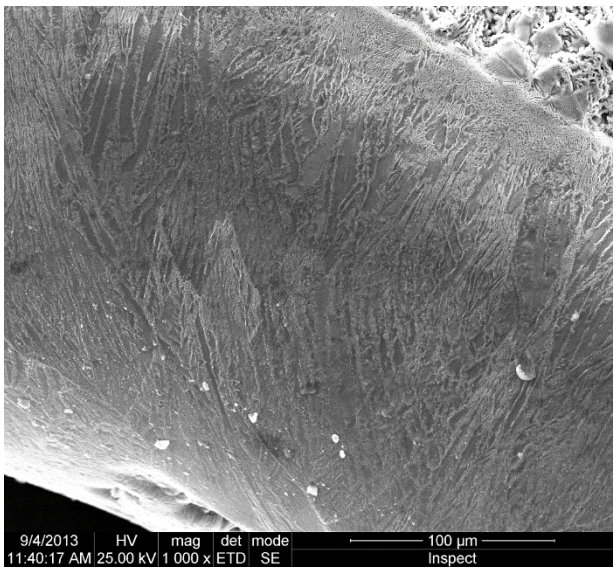

Fig. 14 After LASER interaction

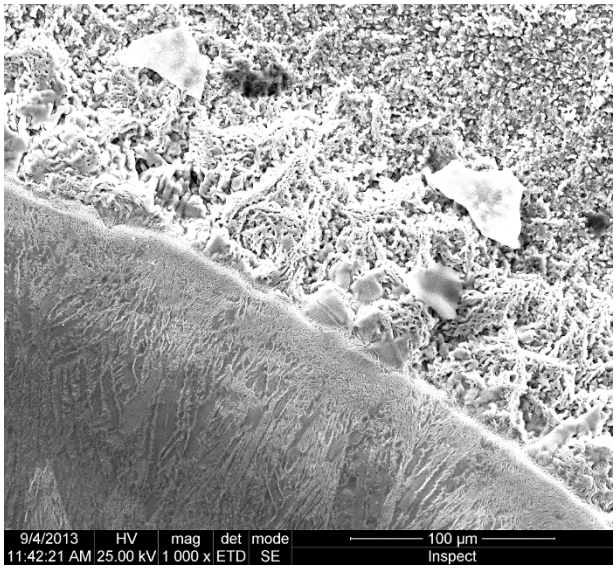

Fig. 15 Fusion zone

Also, we were interested in the average roughness for a sample melted at 10W. The images were taken on the borders of the melted area around which we can observe a constant roughness (approximately 40 nm).

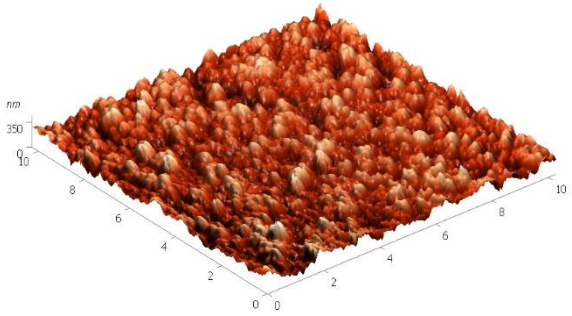

Fig. 16 3D model of the titanium alloy

The pattern and its heights can be observed in the *Fig. 17 2D mapping for roughness*.

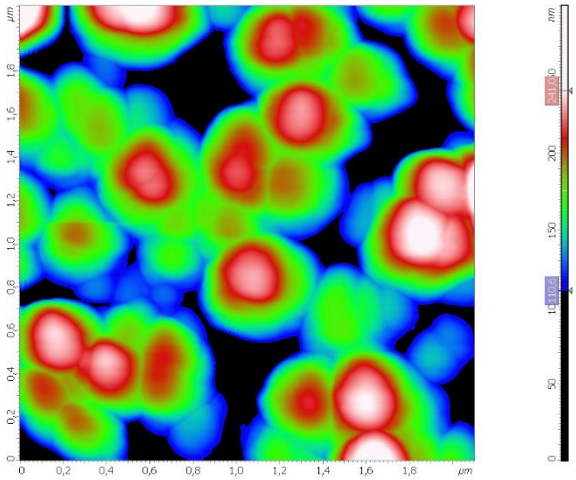

Fig. 17 2D mapping for roughness

OPTICAL MICROSCOPE

Using the optical microscope, we analyzed samples melted at 10 W for 50 seconds.

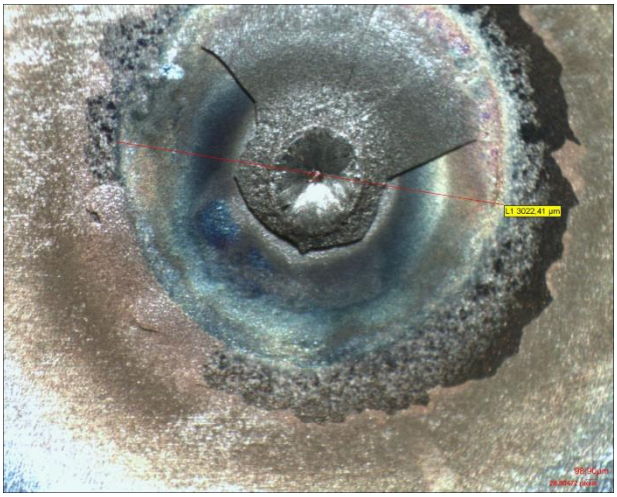

Fig. 18 Melted zone

5. Conclusion

Firstly in the study, we presented a theoretical analysis regarding the heat and fluid flow in a molten pool. Melting procedures were employed for a titanium alloy (Ti6Al4V) as a way to experimentally test the theoretical predictions: LASER light of maximum 25W was focused using a lens at approximately 0.2 mm and aimed at four titanium samples placed at a distance of 60 mm from the lens. Relevant results were obtained for the melted samples since we could observe the dendritic structure, which revealed a columnar geometry. The emergence of this geometry is because under normal gravity conditions the direction of growth for the dendrites is the same as that of the gravitational field. Furthermore, as it can be calculated from Figure 14, the spacing between the dendrites is relevant on a scale of 100µm. X-ray microtomography was also employed in order to determine whether the treated samples presented any microstructural defects. The results reveal that the titanium alloy indeed presents micro-cracks. We also investigated the roughness of the surface (Fig. 17), observing the small inhomogeneity that arose as a result of intricate solidification phenomenon after the laser treatment.

Acknowledgements:

We want to thank for scientific support to:
Ph.D. Professor Mihai Stafe – Politehnica University of Bucharest – Departament of Physics, EUR ING Paul Clark - Durham University
Koen DeBeule – European Space Agency
Junior Researcher Mugurel Balan - Institute of Space Science
Professor Martin Ward – Durham University
Ph.D. Professor Ionelia Voiculescu - Faculty of Engineering and Management of Technological Systems Ph.D. Professor Ionut Cinca – Faculty of Material Sciences and Engineering
Ph.D. Professor Ileana Rau – Department of Chemistry
Ph.D. Professor Cristian Parvu – Department of Chemistry
Cristina Dumitriu – Department of Chemistry
Ph.D. Professor Petrisor Parvu – Faculty of Aerospace Engineering
Ph.D. Professor Dan C. Dumitras – The National Institute for Laser, Plasma and Radiation Physics
Ph.D, Ana –Maria Bratu - The National Institute for Laser, Plasma and Radiation Physics
Mihai Virgil Patachia - The National Institute for Laser, Plasma and Radiation Physics
Professor Corneliu Burileanu – Faculty of Electronics, Telecommunications and IT
Professor Ecaterina Andronescu – Politehnica University of Bucharest
Professor Vasile Bogdan – Politehnica University of Bucharest
Eng. Martin Traub – Fraunhofer Institute for Laser Technology ILT
Eng Jorge Piris – European Space Agency
Professor Ray Sharples – Durham University - Department of Physics
Professor A. Mike Cruise – Royal Astronomical Society, UK
Mr. Iain Carson – LASER 2000

We also want to thank to European Space Agency, Deutsches Zentrum für Luft- und Raumfahrt, Eurolaunch and Swedish Space Center for giving us the opportunity to fly our experiment with REXUS 16 in March 2014.
Also, we want to thank to our sponsors: Royal Astronomical Society, PriceWaterhouseCoopers Romania, Groupama Romania, Farmexpert Romania, TehnoWorld Romania, Durham University, Politehnica University of Bucharest.

Abbreviations

HAZ	Heat Affected Zone
LED	Light-emitting diode
PCB	Printed circuit board
REXUS	Rocket Experiments for University Students
SATP	Standard Ambient Temperature and Pressure
SEM	Scanning Electron Microscope

References for the Abstract

[1] Student Experiment Documentation http://media.wix.com/ugd//6d82a943993f425d946db024d0fbaa37538195.pdf
[2] http://www.rexusbexus.net
[3] Curreri, RA, Lee, JE Stefanescu, DM 1988, Dendritic Solidification of Alloys in Low Gravity, Metallargical Transactions, Volume 19 (11), pp. 2671- 2676